The impact of weld metal creep strength on the overall creep strength of 9% Cr steel weldments

Peter Mayr[a,b,*], Stefan Mitsche[c], Horst Cerjak[b], Samuel M. Allen[a]

[a)] Department of Materials Science and Engineering, Massachusetts Institute of Technology, 77 Massachusetts Av., Cambridge, MA 02139, USA

[b)] Institute for Materials Science and Welding, Graz University of Technology, Kopernikusgasse 24, 8010 Graz, Austria

[c)] Institute for Electron Microscopy and Fine Structure Research, Graz University of Technology, Steyrergasse 17, 8010 Graz, Austria

[*] corresponding author: peter.mayr@tugraz.at; Tel.: +43 316 873 7186

ABSTRACT

In this work, three joints of a X11CrMoWVNb9-1-1 (P911) pipe were welded with three filler metals by conventional arc welding. The filler metals varied in creep strength level, so that one over-matched, one under-matched and one matched the creep strength of the P911 grade pipe base material. The long-term objective of this work was to study the influence of weld metal creep strength on the overall creep behavior of the welded joints and their failure mechanism. Uni-axial creep tests at 600°C and stresses ranging from 70 to 150 MPa were performed on cross-weld samples of all three welds. A total creep testing time of more than 470,000 hours was accumulated. The longest running sample achieved a time-to-rupture of more than 45,000 hours. Creep testing revealed that the use of under-matching weld metal led to premature fracture in the weld metal at higher stress levels. Compared to under-matching weld metal, the use of matching and over-matching filler material increased the time-to-rupture at high stress levels by 75% and 33% at lowest stress levels. At typical component stresses below 100 MPa, all samples failed in the grain-refined heat-affected zone by characteristic Type IV failure. For investigations of the failure modes, cross-sections of fractured samples were investigated by optical light microscopy, scanning electron microscopy and electron backscatter diffraction. The mechanism of weld metal creep failures and Type IV creep failures are discussed in detail.

Keywords: creep resistant steel, creep testing, welded joints, microstructure, Type IV failures.

INTRODUCTION

In recent decades, improved ferritic/martensitic 9-12% chromium steel grades (e.g. P91, P92, P911, P122) as structural materials for high temperature components in thermal power plants have been incorporated in standards, e.g. ASTM A355/A355M-09, introduced to the market. These alloys became widely used in existing thermal power plants by the year 2000. In parallel, the volume of laboratory creep testing data has increased and improved the understanding of creep degradation, especially of the base materials (BM). Long-term creep testing data of weld metals (WM) and cross-welds is still rather scarce. Nevertheless, increasing experience with welded components in-service and data for longer testing of cross-weld samples identified the heat-affected zone (HAZ) of welded joints as the major weak point giving rise to premature failures [1].

Failures in the fine-grained heat-affected zone (FGHAZ) can reduce the creep rupture strength of cross-welds by 50% compared to the plain base metals [2]. Therefore, the first signs of failure, such as void formation, are observed in cross-welds at much earlier stages than in the base materials. These failures in the FGHAZ are categorized as "Type IV cracking" according to a scheme set up by Schüller et al. [3]. The most recent review on Type IV cracking was published in 2006 [4].

In general, Type IV cracking is seen as the result of a zone weak in creep strength surrounded by microstructures that are more creep-resistant, i.e. the coarse-grained HAZ (CGHAZ) and the unaffected base material. This mismatch in creep properties leads to highly complex material behavior which at present is not fully understood [5]. In particular, there is a discrepancy between simulations and observed experimental results. It is well established that at room temperature, by uniaxial in-series tensile loading of cross-welds, the region with the lowest yield strength will try to deform transversely under high strains. If this region is sufficiently thin, it is constrained from deforming by the adjacent stronger areas. As a result, a multiaxial stress state predominates, constrains the weaker region, and prevents it from yielding.

At higher temperatures, in the creep regime,, the situation is more diverse. Li et al. [6] studied the stress-strain distribution in a martensitic P122 weld using a FEM model based on Norton's creep law incorporating four zones with different creep properties: weld metal (WM), coarse-grained HAZ (CGHAZ), FGHAZ, BM. The model results were compared to a Type IV failure observed in a real P122 weld tested at 923K (650°C) for 2,763 hours. Simulation showed that the over-matched WM imposed a constraint on the CGHAZ, and in turn the BM and CGHAZ constrained the FGHAZ. Li et al. concluded that void formation is governed by the equivalent strain and a narrow FGHAZ region is beneficial with regard to reduced void formation. In a similar work, Abe et al. [7] showed experimentally by creep tests up to 10,000 hours that an electron beam (EB) welded

joint of P122 with a reduced HAZ width exhibits twice the lifetime of a standard gas-tungsten-arc-weld. However, final catastrophic fracture of the EB weld also occurred in the FGHAZ by Type IV cracking.
In a recent publication, Bauer et al. [8] reported experimental and finite-element simulation results of a weld configuration similar to the one presented in this work. They concluded that the use of a weld metal with lower creep strength compared to the joined base material creep strength reduces the multiaxiality of the stress state in the Type IV region and thus the accumulation of damage. Consequently, it was predicted that the lifetime of cross-welds can be increased as long as the lower-strength weld metal does not result in premature weld metal failures. All these sources [6-8] suggest a strong influence of constraint on the overall cross-weld strength.

On the other hand, an alternative approach to model Type IV damage in creep resistant steels was introduced by Kimmins and Smith [9], who suggested that constraint is relaxed by grain boundary sliding. Their simulations showed good agreement with experimental studies and they concluded that the weak Type IV zone experiences no measureable constraint from adjacent stronger materials. Sawada et al. [10] contributed to this discussion by investigating some of the fractured P911 cross-welds of this work using transmission electron microscopy (TEM), concluding that the higher multiaxiality of stress state in the center of the specimen did not affect the dislocation structure and the growth rates of $M_{23}C_6$ carbides during creep. On the other hand, multiaxiality promoted the formation of Z-phase. Regardless of the stress state, the FGHAZ showed an increased coarsening rate for $M_{23}C_6$ carbides, a higher number density of Z-phase particles and a decrease of dislocation density compared to the base material microstructure.

Motivated by this contradictory data in literature, the identification of the influence of weld metal strength (i.e. the level of constraint) on the overall long-term creep behavior of P911 cross-welds became the objective of this study. Three P911 cross-welds with three weld metals differing in creep strength were fabricated and creep tested at 650°C up to 45,000 hours.

EXPERIMENTAL

Materials

In this investigation, four sections of seamless pipe of ASTM Grade P911 (ASTM A355/A355M-09)[1] with an outside diameter of 355 mm and a wall thickness of 43 mm were joined by butt-welding.

Table 1: Specification of chemical composition (wt.%) of base material and weld filler metals.

	C	Si	Mn	Cr	Ni	Mo	V	W	Nb	N	B
ASTM A335-P911 pipe X11CrMoWVNb9-1-1	0.12	0.20	0.47	8.62	0.24	0.94	0.20	0.96	0.084	0.012	0.018
E CrMo91 B 4 2 H5 ASTM A335-P91-type	0.09	0.20	0.60	9.00	0.80	1.10	0.20	-	0.05	0.04	-
W ZCrMoWVNb911 ASTM A335-P911-type	0.11	0.20	0.60	8.80	0.70	1.00	0.20	1.00	0.05	0.05	-
W ZCrMoWVNb9 0.5 1.5 ASTM A335-P92-type	0.11	0.20	0.60	8.80	0.70	0.5	0.70	1.60	0.05	0.05	-

P911 pipe base material was received in normalized and tempered condition and showed a tempered martensitic microstructure. A different filler material was used for each of the three joints (see Table 1),.

- Joint 1 was welded with E CrMo91 B 4 2 H5 (ASTM A355 - Grade P91) weld metal. Grade 91 weld metal under-matches the creep properties compared to the mean P911 base metal creep strength.
- Joint 2 was welded using W ZCrMoWVNb911 (ASTM A355 - Grade P911) weld metal which is of matching creep strength compared to P911 base material.
- Joint 3 was fabricated using W ZCrMoWVNb9 0.5 1.5 (ASTM A355 - Grade P92) weld metal which over-matches the creep properties compared to P911 base material.

In the absence of weld metal creep rupture data, the 100,000 hour base material creep rupture strength at 600°C based on ECCC evaluations of grade P91, P911 and P92 are taken as 86 MPa, 98 MPa, and 113 MPa, respectively [11]. A schematic of the four pipe sections welded with three different weld filler metals is shown

[1] In European standards this is designated X11CrMoWVNB9-1-1 (E911, EN-10302-2002).

in Figure 1. The chemical composition of the pipe material \and weld metal chemistries as published by the manufacturer [12] are given in Table 1.

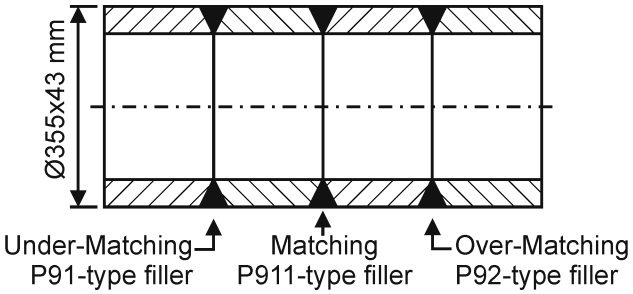

Figure 1: Schematic of the welding setup of four P911 pipe sections using three different filler metals differing in creep strength.

Welding Procedure

The root beads of all three joints on the pipe were made by means of gas-tungsten arc welding (GTAW) with a Ø2.4 mm wire. For subsequent layers shielded-metal arc welding (SMAW) was utilized, using electrodes with diameters of Ø2.5, 3.2 and 4.0 mm. Voltage, current, and welding speed were the same for all three welds, resulting in a comparable heat input. Pre-heat temperatures and inter-bead temperatures were kept in the range of 200-300°C (473-573 K) at all times. Figure 2 shows a sketch of the weld groove geometry and the applied welding sequence for the three butt welds. All three welds were exposed to a post-weld heat treatment at 760°C (1033 K) for two hours. Further details regarding the welding procedure can be found in [13].

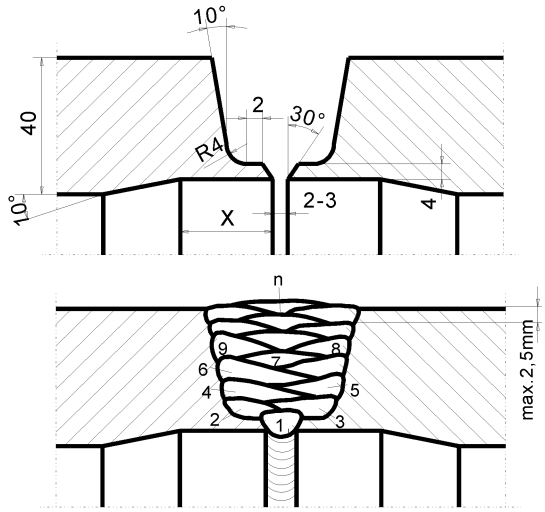

Figure 2: Weld groove geometry and applied welding sequence for all three butt welds. [13]

Creep Testing

For long-term creep testing of the three weldments, cross-weld specimens were machined out of the joints perpendicular to the welding direction. Each creep specimen included weld metal in the center of the specimen flanked by the heat-affected zones and unaffected base material (see Figure 3). To establish creep elongation data, each specimen was fabricated with ridges to measure the change of the reference length L_0. Uni-axial creep tests were performed at 600°C (873 K) using multi-specimen vertical dead-weight creep testing machines. Up to 9 specimens were mounted in a row and the stress of each specimen was adjusted through its gauge diameter d_0. A parametric drawing of a creep test specimen is given in Figure 3.

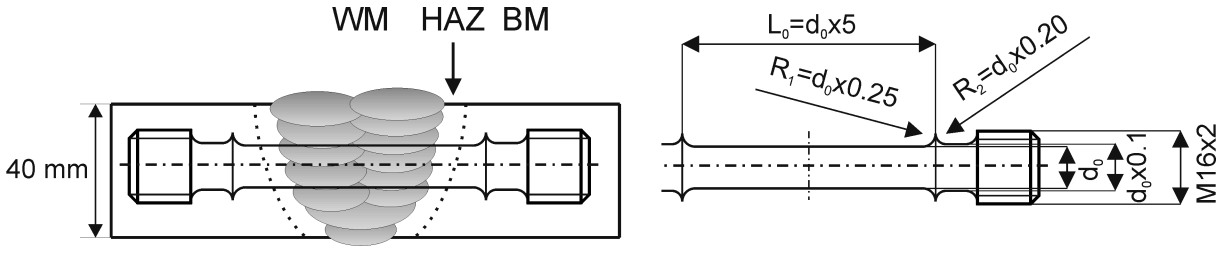

Figure 3: Schematic of the specimen location within the butt-welded joint (left) and parametric drawing of a creep specimen with ridges for integral strain measurement. Reference length L_0 and diameters are adjusted according to the applied force and the desired stress level.

A minimum gauge diameter of 7 mm was required to eliminate unreliable creep testing data from smaller sized specimens. Testing stresses ranged from 70 MPa to 150 MPa. Specimen designation includes the tested weld and the testing stress, e.g. UM120 describes a specimen containing the under-matching weld metal exposed to 120 MPa. Creep elongation was measured for all specimens during interruptions of the creep tests at discrete time intervals. To avoid unwanted excess straining of the specimens during cooling and heating, specimens where only loaded when they were at testing temperature. The measured integral creep strain represents the strain observed over the whole gauge length including weld metal, HAZ, and base material. Therefore, the measured strain data cannot be allocated to a special region within the gauge length but represents the integral accumulated creep strain of the entire cross-weld. The creep testing procedure is in accordance with DIN EN 10291-2001 and recommendations given by the European Creep Collaborative Committee - ECCC [14].

Investigation of Failure Mode

To determine the location of failure and the failure mode, cross-sectional metallographic specimens along the specimen axis were prepared for each creep specimen. After slight grinding, etching the specimen surface with 25 ml distilled water, 50 ml hydrochloric acid, 15 g iron (III) chloride and 3 g ammonium tetrachlorocuperate II (Adler-etchant) revealed the weld metal structure, heat-affected zone and unaffected base material.

Additionally, metallographic specimens for light optical microscopic investigations were prepared. After polishing to a 1 µm surface finish and etching using 100 ml distilled water, 0.75 g ammonium hydrogen fluoride and 0.90 g potassium disulfide (modified LBII etchant) digital images were recorded using a Reichert MeF3 optical microscope.

Scanning electron microscopy was performed on either polished or additionally etched specimens using a 100 ml ethanol, 10 g picric acid and 2 ml hydrochloric acid solution (Picric acid + HCl). Operating parameters of the SEM are documented in the legend of each image.

Electron backscatter diffraction (EBSD) was performed on samples vibration polished down to 0.02 µm finish. EBSD data was obtained using a XXXX equipped with a XXXX.

RESULTS AND DISCUSSION

Cross-weld Creep Strength

In total, a creep testing time of more than 470,000 hours accumulated for all specimens. Longest running individual tests reached more than 45,000 hours. Figure 4 shows the creep rupture data in a double logarithmic

stress versus time plot. Cross-weld creep data are compared to the mean creep strength of P911 base material and a ±20% scatter band [11]. Figure 4b shows the change from high strain rate tests at high stresses to characteristic creep behavior at medium and low stresses displaying a pronounced three-stage creep behavior.

At the highest stress level of 150 MPa, the specimens failed in the sequence under-matching, matching and over-matching weld. The time-to-rupture ranged from 1,314 hours (UM150) to 2,311 hours (OM150). All three specimens showed slightly earlier failures compared to the mean P911 base material testing data. Basically, at stress levels higher than 100 MPa, all cross-welds failed within the -20% scatter band limit of the base material. Data plotted in Figure 4 also reveals that an extrapolation of creep rupture times based on testing results below 10,000 hours would lead to a significant over-estimation of acceptable stresses. A steep drop in creep rupture strength is observed for all specimens beyond the 10,000 hour mark.

For long-term tests beyond 10,000 hours, the sequence of failed welds changed, showing the under-matching specimens failing first, followed by the over-matching and matching specimens. This sequence prevails to lowest testing stresses and longest testing times. The present results agree with [6] by indicating a some strengthening of cross-welds when a weld metal of similar or over-matching creep strength is used. This effect is more pronounced at high stresses and shorter testing times, e.g. an increase of time-to-rupture at 150 MPa between the UM150 and the OM 150 specimens of +75%. At lower stress levels, this advantage decreases and increases the lifetime of cross-welds from 33,997 hours (UM70) to 45,374 hours (M70) by 33%. Contradictory, the use of an over-matched weld metal does not further increase the time-to-rupture of cross-welds which is in accordance with simulation results in [8]. The over-matching specimen tested at 70 MPa (OM70) failed after 41,039 hours, slightly earlier (-3.6%) relative to the matching specimen (M70).

Because the same welding procedure was used on each specimen, the length scales of the HAZ regions of all three welds should be similar. Therefore, the observed strengthening or restraining effect should be attributed to the weld metal and executed by the unaffected base material and the higher strength weld metal. This confirms the numerical simulation results in [6], which predicted a restraint of the CGHAZ by the weld metal and a restraint of the FGHAZ by the CGHAZ and the unaffected base material. The predicted strengthening accompanied by an increase in time-to-rupture of cross-welds through the use of a weld metal of lower creep strength in [8] could not be confirmed. In the investigated stress range, all under-matching specimens failed first.

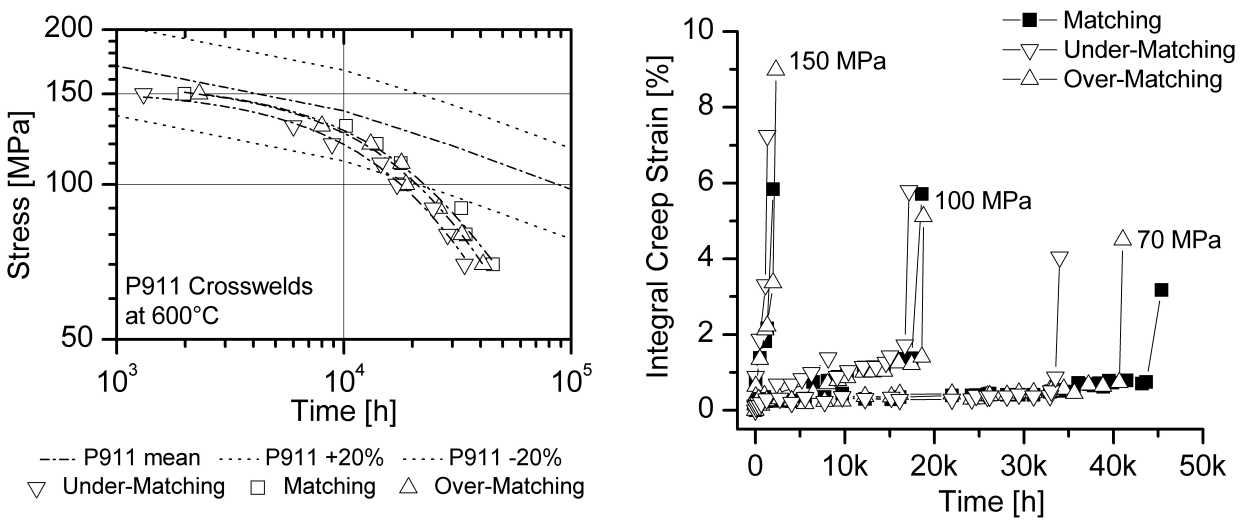

Figure 4: Creep rupture strength of P911 cross-weld specimens at 600°C compared to the mean P911 base material creep strength [11] and its ±20% scatter band (left). Accumulated creep strain as a function of time for low, medium and highly stressed specimens of the three welds.

Location of Failure

Optical micrographs of cross-sectional cuts of all creep specimens revealed that catastrophic failure either occurred in the weld metal or in the heat-affected zone.

Based on the results from all welds, a transition from weld metal failures at high stresses, to HAZ failures at lower stresses is observed. The transition stress level at which this change occurs depends on the weld metal. For the under-matching weld, this stress is between 100 MPa and 110 MPa, whereas for the matching weld it is between 130 MPa and 150 MPa. All specimens of the over-matching series fractured within the HAZ which suggests that the transition is at even higher stresses beyond 150 MPa. These results confirm that at characteristic design stresses for power plant components lower than 100 MPa, only HAZ failures are to be expected.

Figure 5 shows the two observed failure locations on two representative specimens tested at 120 MPa. The specimen of the under-matching weld (UM120) shows a failure in the weld metal in which the crack is perpendicular to the specimen axis, i.e. the loading direction, in the lower half of the specimen and follows the weld bead geometry in the upper part of the specimen. The matching weld (M120) failed in the HAZ and the failure is completely parallel to the weld fusion line. Creep rupture elongation (RE) is very similar for both specimens with 5.3% for UM120 and 3.0% for M120 and so is the reduction of area after fracture (RA) with

11.0% and 9.8% respectively. Table 2 summarizes the obtained creep testing data for all specimens including failure location, reduction of area (RA) and rupture elongation (RE). In general, the reduction of area is very low indicated by a mean value of 5.5% and a single standard deviation of 5.5. Rupture elongation decreases with time as visible in Figure 4b. Elongation values are also low with a mean value of 4.3% and a single standard deviation of 2. Therefore, most of the failures can be categorized as macroscopically brittle. No statements on the microscopic ductility, i.e. ductility of individual grains, in the failed regions can be made based on these data.

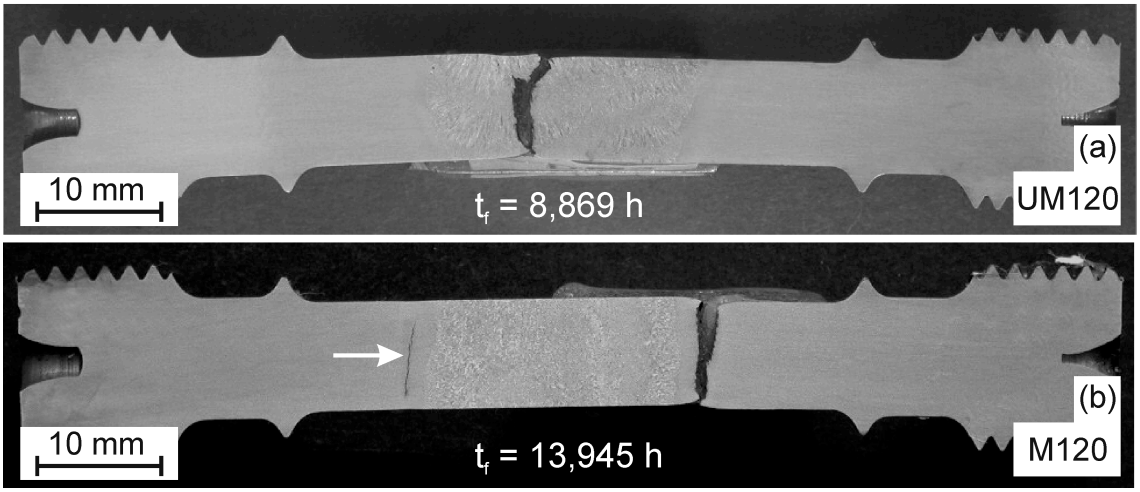

Figure 5: Creep fracture in the weld metal of an under-matching specimen tested at 120MPa at 600°C (873K) (a), and in the heat-affected zone of the equivalent matching specimen (b). The white arrow in (b) marks a region in the left HAZ where damage has progressed to severe cracking.

Table 2: Summary of creep testing results at 600°C (873K) for cross-welds of P911 welded joints.

	Spec.	Stress Level [MPa]	Time to rupture [h]	Fracture Location	RA [%]	RE [%]
Under-Matching	UM150	150	1.314	WM	18.4	7.3
	UM130	130	5.982	WM	9.0	5.4
	UM120	120	8.869	WM	11.0	5.3
	UM110	110	14.519	WM	13.9	8.1
	UM100	100	17.145	HAZ	9.1	5.8
	UM90	90	24.680	HAZ	11.0	1.0
	UM80	80	28.613	HAZ	1.1	2.6
	UM70	70	33.977	HAZ	6.8	4.1
Matching	M150	150	1.988	WM	13.0	5.8
	M130	130	10.226	HAZ	9.3	3.6
	M120	120	13.945	HAZ	9.8	3.0
	M110	110	17.819	HAZ	8.4	1.4
	M100	100	18.578	WM		5.7
	M90	90	32.913	HAZ	1.3	4.1
	M80	80	34.446	HAZ	6.5	4.2
	M70	70	45.374	HAZ	7.7	3.2
Over-Matching	OM150	150	2.311	HAZ	27.9	9.0
	OM130	130	7.992	HAZ	10.4	2.9
	OM120	120	13.150	HAZ	11.8	2.8
	OM110	110	17.931	HAZ	9.2	1.4
	OM100	100	18.786	HAZ	5.3	5.1
	OM90	90	26.185	HAZ	6.1	2.8
	OM80	80	33.062	HAZ	5.5	3.8
	OM70	70	41.039	HAZ	4.9	4.5

RA … Reduction of area RE … Rupture elongation

WM...Weld metal HAZ.. Heat affected zone

FAILURE MORPHOLOGIES

Weld Metal Failures

The weld metal itself in a multi-layer weld is characterized by several different microstructures on a very small length scale. Due to the thermal influence of the subsequent deposition of weld beads on already solidified beads, a variety of microstructures can evolve. The uninfluenced solidified weld metal shows elongated columnar grains which have grown during solidification in the direction of the maximum temperature gradient (see Figure 6a). The grain boundaries of these columnar grains usually show an increased level of segregation. In this investigation they exhibit an increased susceptibility to crack formation as can be seen in Figure 6b. Cracks preferably form along the boundaries between columnar grains which are oriented perpendicular to the applied load. Additionally, due to the length of such grain boundaries of several millimeters or 2/3 of the specimen thickness, cracks can grow relatively easy without hitting significant obstacles.

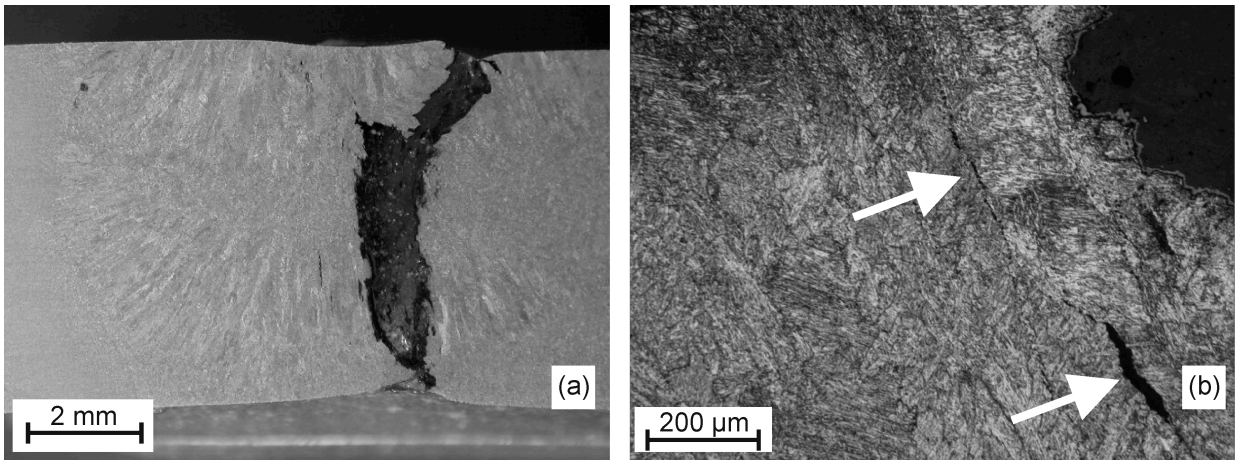

Figure 6: Optical micrographs of a weld metal failure in the under-matching weld specimen tested at 600°C (873K), 120 MPa (UM120) for 8,869 hours revealing fracture and secondary cracking along the columnar grains of solidified weld metal.

On the other hand, in regions where the initial solidification microstructure has been refined through deposition of subsequent beads, an equiaxed grain structure of different grain size is formed (Figure 7) similar to the formation of the heat-affected zone microstructure. In such refined weld metal, creep damage occurs by voiding. Voids (r-type) [15] predominantly form at prior austenite grain boundaries perpendicular to the loading direction. Figure 7b shows a SEM image of a grain in the weld metal where voids formed predominantly along the prior austenite grain boundary and interlinkage leads to the formation of micro cracks.

Once micro-cracks have connected and formed macroscopic cracks, catastrophic failure occurs. The sequential formation of voids, followed by microscopic and macroscopic cracks, continuously increases the stress in the remaining load carrying cross section.

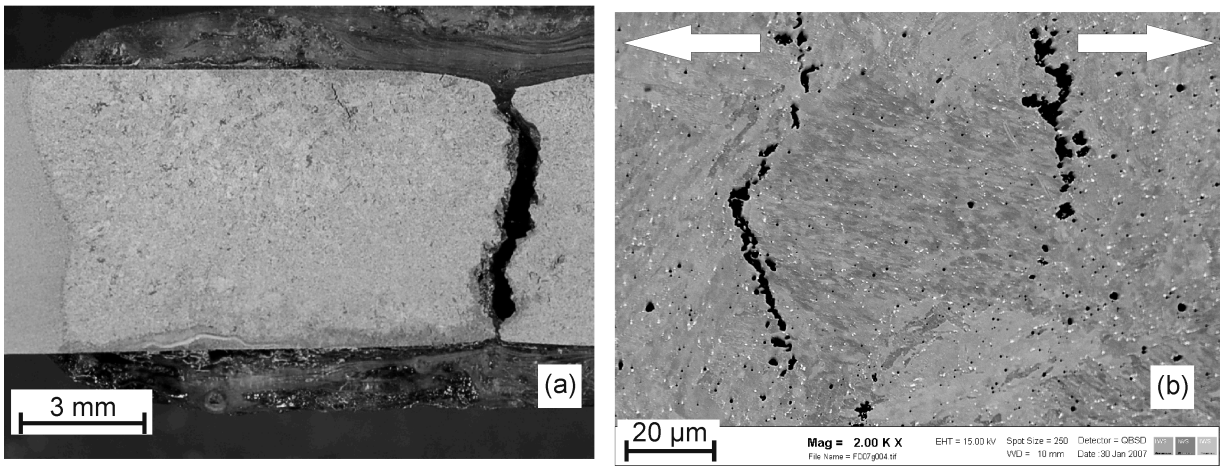

Figure 7: Optical micrograph of a weld metal failure in the under-matching weld specimen tested at 600°C (873K), 130 MPa (UM130) for 8,982 hours showing fracture in the refined weld metal (a) by creep cavitation preferably along prior austenite grain boundaries perpendicular to the loading direction (b).

Heat-Affected Zone Failures

Fracture in the heat-affected zone of cross-weld specimens always occurred absolutely parallel to the weld fusion line as documented in Figure 5b. The voids and micro cracks that formed in the unfractured HAZ of specimen M120 (Figure 5b) allowed a closer look at the progression of failure at lower stresses in the HAZ. SEM investigation (Figure 8) showed that voiding is a very localized phenomenon limited to an area about 1 mm in width close to the unaffected base material and closely parallel to the weld fusion line. As damage progresses, voids have interlinked and formed micro cracks. As in the fine-grained weld metal failures, once the remaining load-bearing cross-section was weakened, catastrophic failure occurred. At higher magnification (Figure 8b), a uniform fine-grained microstructure with a prior austenite grain size below 5 µm is visible. Bright spots indicate coarse precipitates mainly aligned along the grain boundaries.

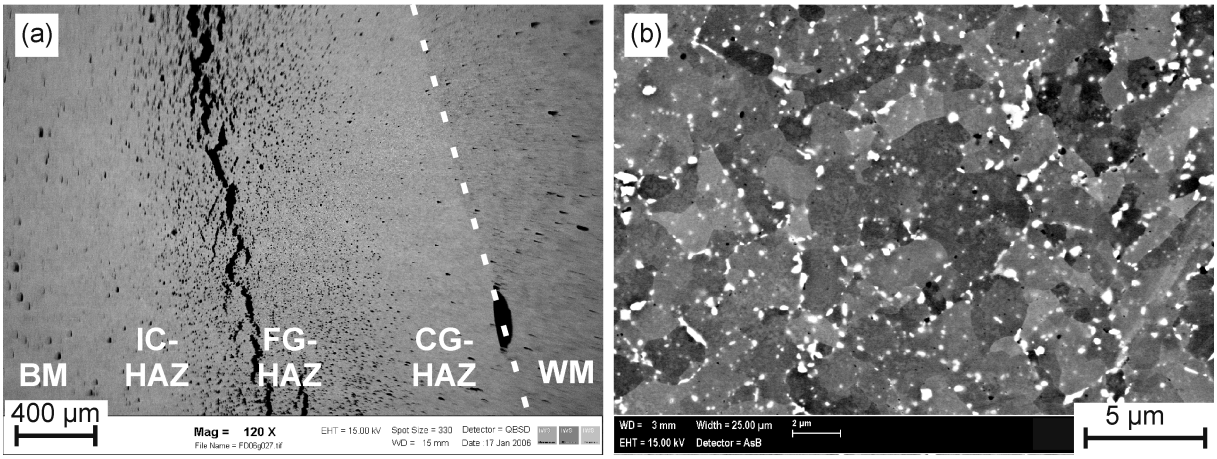

Figure 8: SEM image of void distribution in a matching series specimen (M120) fractured after 13,945 hours at 120 MPa (a). SEM image at higher magnification of the fine-grained region in specimen M120 (b).

Through energy-dispersive X-ray spectroscopy (EDX), coarse particles were identified as mainly Mo-rich Laves phase (Fe_2Mo) and Cr-rich carbides ($M_{23}C_6$). These hard second-phase particles can act as initiation sites for creep voids. An inverse pole figure of the fine-grained region confirmed the small grain size in this region and additionally revealed the absence of a martensitic lath structure.

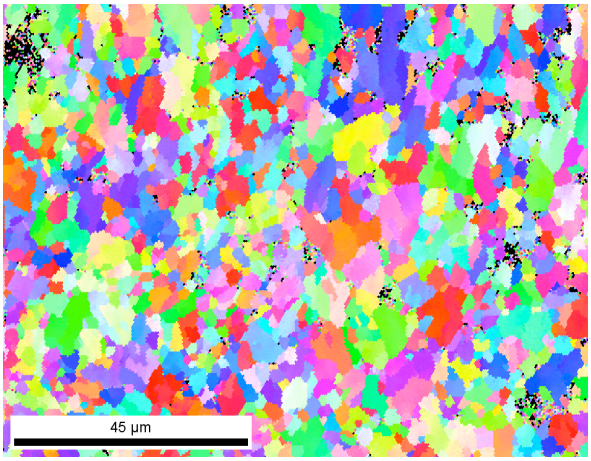

Figure 9: Inverse pole figure of an area close to the failed region in specimen M120. Clusters of black pixels indicate locations of voids.

Considering the most potent high-temperature strengthening mechanisms in martensitic creep resistant steels, i.e., a martensitic lath structure and finely dispersed small-sized particles, this fine-grain, equiaxed microstructure is highly susceptible to premature creep failures.

Microstructural investigations of all HAZ failures confirmed that all occurred in the fine-grained region, classifying them as characteristic Type IV failures. Independently of the weld metal creep strength, Type IV cracking in the fine-grained heat-affected zone is the life-limiting failure mechanism of all three welds at stress levels below 100 MPa.

SUMMARY AND CONCLUSIONS

Within this investigation, the influence of weld metal creep strength on the overall creep performance of grade 911 cross-welds was investigated. Four sections of a P911 pipe were joined by three welds with three different weld filler metals. The filler metals varied in creep strength level, so that one over-matched, one under-matched and one matched the creep strength of the P911 grade pipe base material. Long-term creep testing of cross-weld specimens at 600°C (873K) revealed the time-to-rupture at different stress levels. After fracture, creep specimens were investigated by optical and electron microscopy regarding failure location and failure mode.

From the results of this work it can be concluded that:

- At lower stress levels (<100 MPa), corresponding to realistic design stresses for real power plant components, failure occurs consistently in the fine-grained heat-affected zone by Type-IV cracking.
- At higher stress levels, failures occur in the weld metal by either cracking along elongated columnar grain boundaries or voiding preferentially along prior austenite grain boundaries oriented perpendicular to the applied load.
- The change of failure location from weld metal to HAZ failures is governed by the weld metal creep strength. Joints with weld metal of lower strength show a lower transition stress while higher strength weld metals also at higher stress levels force the failure into the HAZ.
- Type IV failures are characterized by extensive creep void formation exclusively in the fine-grained heat-affected zone. This HAZ region is highly susceptible to Type IV-failures, as from the beginning of creep testing an equiaxed grain structure is present with a very small average grain size (< 5µm) and no martensitic lath structure. The higher area fraction of grain boundaries in this region favors accelerated short-circuit diffusion which leads to accelerated recovery, coarsening of precipitates and therefore in a drop of creep strength.

ACKNOWLEDGMENTS

This work was part of the Austrian research cooperation "ARGE ACCEPT – COST 536" and was funded by the Austrian Research Promotion Agency (FFG) which is gratefully acknowledged. PM likes to acknowledge the support of the Austrian Academy of Sciences and the Max Kade Foundation.

References

[1] S. J. Brett, UK experience with modified 9Cr (grade 91) steed, in: J. Veivo, P. Auerkari (Eds.), Baltica VII: Life Management and Maintenance for Power Plants, Vol 1, vol 246, 2007, pp. 48-60.
[2] M. Tabuchi, Y. Takahashi, Evaluation of creep strength reduction factors for welded joints of modified 9CR-1MO steel (P91), in: Vancouver,BC, Canada, 2006, pp. 1-6.
[3] H. J. Schueller, L. Hagn, A. Woitscheck, Der Maschinenschaden 1 (1974) 1-13.
[4] J. A. Francis, W. Mazur, H. K. D. H. Bhadeshia, Materials Science and Technology 22 (2006) 1387-1395.
[5] D. J. Smith, N. S. Walker, S. T. Kimmins, Type IV creep cavity accumulation and failure in steel welds, in: International Journal of Pressure Vessels and Piping, vol 80, Elsevier Ltd., 2001, pp. 617-627.
[6] D. Li, K. Shinozaki, H. Kuroki, Materials Science and Technology 19 (2003) 1253-1260.
[7] F. Abe, M. Tabuchi, Science and Technology of Welding and Joining 9 (2004) 22-30.
[8] M. Bauer, E. Roos, A. Klenk, K. Maile, Engineering Fracture Mechanics In Press, Corrected Proof.
[9] S. T. Kimmins, D. J. Smith, Journal of Strain Analysis for Engineering Design 33 (1998) 195-206.
[10] K. Sawada, M. Bauer, F. Kauffmann, P. Mayr, A. Klenk, Materials Science and Engineering a-Structural Materials Properties Microstructure and Processing 527 (2010) 1417-1426.
[11] ECCC Datasheets - GX12CrMoVNbN9-1, X11CrMoWVNb9-1-1, ASTM Grade 92, in: European Creep Collaborative Committee - Working Group 3A, 2005.
[12] Weld Consumable Datasheets - Thermanit MTS3, Thermanit Chromo 9V, Thermanit MTS 616, Thermanit MTS 911, in: Böhler Schweisstechnik Deutschland, 2005.
[13] P. Mayr, H. Cerjak, C. Jochum, e. al., Proceedings of the ASME Pressure Vessels and Piping Conference 2007, Vol. 9 (2008) 690.
[14] A. Klenk, B. Buchmayr, ECCC Recommendations - Volume 3 Part II - Data Acceptability Criteria and Data Generation: Creep Data of Welds, in: 2005.
[15] M. E. Kassner, Fundamentals of creep in metals and alloys, Elsevier, Oxford, 2009.